Solid State Phenomena
ISSN: 1662-9779, Vol. 343, pp 9-14
doi:10.4028/p-eu98j0

Submitted: 2022-09-02
Revised: 2022-12-01
Accepted: 2022-12-04
Online: 2023-05-30

Prevention of Bunched Basal Plane Dislocation Arrays in 4H-SiC PVT-Growth

J. Steiner[1,a], B. D. Nguyen[2,b], S. Sandfeld[2,c], P. J. Wellmann[1,d*]

[1]Crystal Growth Lab, Materials Department 6 (i-meet), FAU Erlangen-Nürnberg, Martensstr. 7, D-91058 Erlangen, Germany

[2]Research Center Jülich Institute for Advanced Simulation, Wilhelm-Johnen-Str., D-52428 Jülich, Germany

[a]johannes.steiner@fau.de, [b]bi.nguyen@fz-juelich.de, [c]s.sandfeld@fz-juelich.de, [d]peter.wellmann@fau.de

Keywords: X-ray topography, physical vapor transport, numerical modeling, stress, basal plane dislocations

Abstract. To prevent arrays of basal plane dislocations (BPD) forming during grown 4H-SiC single crystals, the growth cell in physical vapor transport (PVT) growth was modified by adapting the temperature gradients, the seed attachment method and the seeding phase. The resulting reduction in stress was modeled numerically and the crystals were investigated by X-ray topography (XRT) and molten potassium hydroxide (KOH) etching. Due to these modifications, the formation of BPD arrays was completely suppressed.

Introduction

Silicon Carbide (SiC) matured to be one of the most important wide bandgap semiconductor for the use in power electronics [1]. State of the art 4H-SiC crystals for the use in power electronics are grown with the physical vapor transport method (PVT) and exhibit a largely micropipe-free quality as well as densities of threading screw (TSD) and threading edge (TED) dislocations in the order of $<10^3$ cm^{-2} and $<10^5$ cm^{-2}, respectively. Basal plane dislocations (BPDs), known for increasing the leakage current in MOSFETs or JFETs [2, 3], are reduced to densities as low as $<10^3$ cm^{-2}. BPDs are known to be generated by thermoelastic stress, TSDs terminating at the $(000\bar{1})$-facet and, more specifically, can arise from the shoulder region of the crystal during growth [4-6]. Nakano et al. reported a distinct distribution of BPDs in an array-like manner and proposed a model for the generation of these arrays. The authors explain the occurrence of the arrays with a generation of bunched BPDs at the crystal shoulder region, based on the numerical modeling of Gao et al. covering BPD multiplication [7]. Gao et al. demonstrates a connection between the curvature of the growth front of a SiC crystal and the resulting BPD defect density. The more the crystal growth interface is curved, a higher amount of stress is induced during the growth phase. By flattening the convex shape of the growth interface during PVT-growth, the BPD density and the amount of BPD arrays should be reduced. In addition, finely tuned process parameters such as temperature gradients or the method of the seed attachment are implemented to further reduce stress during and after the growth process. In an earlier work it was demonstrated that an inhomogeneous doping concentration during the seeding phase will increase the amount of stress present in the crystal [8].

The aim of this work is to reduce the amount of BPD arrays with the help of modifications to the process parameters and growth cell. The modifications will concentrate on reducing radial and axial temperature gradients present in the crystal, flattening the shape of the growth interface, insure that the doping concentration during the seeding phase changes as little as possible and decreasing the amount of stress introduced by graphite parts such as the crucible wall and seed holder. To achieve this, two crystals A and B are grown using the PVT method. After growth, two wafers A1 and B1 were cut close to the crystal's cap. Both wafers were characterized by X-ray topography (XRT) and Raman-spectroscopy. To verify the defect character of the bunched array, wafer A1 was KOH-etched. To estimate the impact of the modifications on the stress in the resulting crystal, numerical

calculations were conducted, including stress introduced by temperature gradients present in the crystal and also differing thermal coefficients of expansion due to material and doping concentration.

Experimental

Two 4H-SiC crystals A and B of 100 mm diameter were grown via the PVT method with similar growth parameters such as pressure, nitrogen doping and growth temperature. The growth pressure was set between 5 and 30 mbar, and the temperature was maintained between 2050-2100°C, measured on top of the graphite crucible. The nitrogen flux was ramped up from zero during the initial decrease of ambient pressure to growth pressure, reaching 5% of the argon's gas flux. This was done to compensate for additional residual nitrogen releasing from the graphite isolations during the seeding phase of the growth process, resulting in a smooth transition of the doping concentration between the seed and the newly grown crystal. The doping ramp was the same for crystal A and B. Additionally, the seed used for the growth of crystal B was taken from crystal A. This way the seed exhibited a doping level similar to the one expected to be present in crystal B. Both seeds for crystal A and B exhibited a 4° off-axis angle towards the $<11\bar{2}0>$ direction.

The hot zone of crystal B has been modified to temperature gradients responsible for the degree of the convex shape of the growth interface. The axial temperature gradient inside crystal A was calculated to be 33 K/cm, while the changes for the growth of crystal B resulted in an axial temperature gradient of 25 K/cm. The radial temperature gradients are calculated to be 4.0 and 1.8 K/cm for crystal A and B, respectively. Furthermore, the seed holder's thickness was reduced down to 15% of the original thickness. In addition, for crystal B the growth cell was modified in such a way that the crystal's side wall was not connected to the graphite parts of the crucible, therefore preventing stress introduced during the cooldown phase of the growth. An overview of the process parameters is depicted in table 1.

Table I. Overview of process parameters and modifications to the growth cell of crystal A and B.

	Growth temperature [°C]	Initial doping ramp	Contact to side wall	Seed holder's thickness	Axial T-grad. [K/cm]	Radial T-grad. [K/cm]
Crystal A	2100	yes	yes	100%	33	4.0
Crystal B	2055	yes	no	15%	25	1.8

After the growth, both crystals A and B were sliced and polished. To investigate the bow of the basal plane and the occurrence of BPD arrays in the crystal, XRT measurements of the wafers A1 and B1 closest to the crystal cap were carried out by the Fraunhofer department IISB in Erlangen (Germany), employing a Rigaku XRTmicron advanced X-ray topography setup. All sliced wafers from both crystals were investigated regarding their optical phonon-plasmon coupled (LOPC) mode's peak position utilizing a Horiba LabRAM HR Evolution confocal Raman microscope. For this, a 532 nm laser was utilized in combination with an 1800 gr/mm grating and a magnification of 100 times. The LOPC's peak position was used to approximate the doping concentration [9]. Since the nitrogen doping level influences the coefficient of thermal expansion (CTE) of 4H-SiC [10], this measurement is relevant to improve the accuracy of the numerical calculation of stress present in the crystal. This way the doping concentration of the complete crystal can be approximated and included into the numerical simulation.

Finally, wafer A1 was etched with molten potassium hydroxide (KOH) at 520°C for 5 min with our in-house FAU etching setup to verify the type of defects forming the observed arrays in the XRT measurements.

Results and Discussion

Figure 1a and b depicts X-ray images taken from crystal A and B inside the graphite crucible, after crystal growth was concluded. The growth interface of crystal A is characterized by a pronounced convex shape, resulting in a crystal cap mainly characterized by the shoulder region. In comparison, the cap of crystal B is mainly exhibiting a flat growth interface with a small shoulder region at the edge of the crystal. According to Nakano et al., less stress should be introduced by the shoulder region. This assumption is validated by the XRT measurements.

Figure 1c shows the results of the numerical calculation, more specifically the shear stress present in the crystal. The data set draws a line from the center of the crystal to the edge, at the same position where the respective wafers A1 and B1 are taken from. The calculated stress decreases from a maximum of 18.0 MPa in case of wafer A1 to a maximum of 8.3 MPa in case of wafer B1 as a result of the modified seed attachment method, the changes in the hot zone and the homogeneous nitrogen doping concentration.

Figure 2 depicts the XRT measurements taken with a $11\bar{2}0$ reflex from wafer A1 and B1, respectively. Wafer A1 clearly exhibits defect arrays lying perpendicular to the off-cut direction of the wafer. The defects making up these arrays are identified to be of the BPD type, as seen in the inset of Figure 2a and also more clearly in Figure 3b. The distance between the arrays was measured and calculated to be 0.38 ± 0.10 mm along the c-axis, a similar magnitude as reported by Sonoda and Nakano [4, 6]. On the other hand, the XRT measurement of wafer B1 doesn't depict any kind of arrays. There is a cluster of micropipes (MP) present in the center of both wafers. These were introduced during the growth of crystal A and consequently reintroduced to crystal B since a wafer from crystal A was used as a seed to grow crystal B. The white areas in Fig. 2a and 2b are a result of the basal plane's bow. While we also conducted additional measurements with a 0008 reflex, wherein the white area was smaller and still no BPD arrays could be observed, it cannot be fully ruled out that in this area there are some BPDs arrays of weak intensity hidden on wafer B1. Also, next to the MP cluster in the center a medium sized area of stacking faults is visible in wafer B1. With the help of the XRT measurements, the bow of the basal plane in wafers A1 and B1 was determined and amounts to 12 m and 26 m, respectively. Although 26 m is still a comparatively high amount of bow, the reduction in regard to wafer A1 is apparently enough to prevent the formation of BPD arrays. The overall BPD density of wafer A1 was approximated to be $>10^4$ cm^{-2} while the density of BPDs in wafer B1 was lowered by one magnitude to be in the range of $10^3 cm^{-2}$.

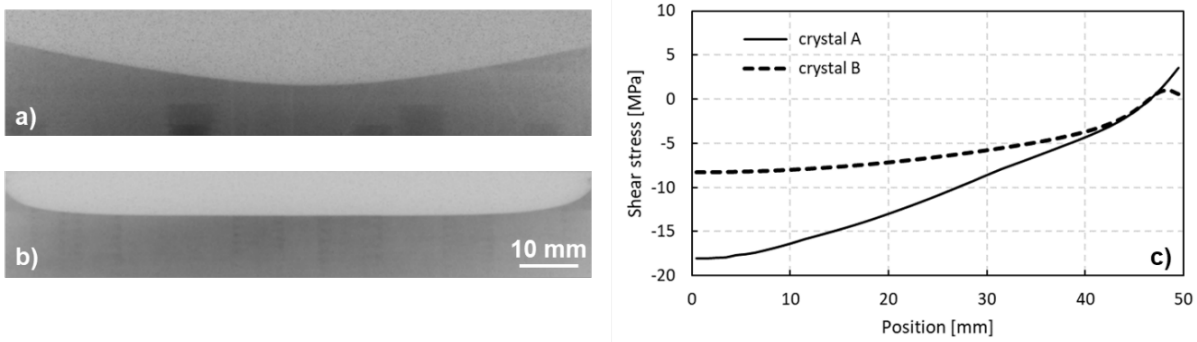

Fig. 1. X-Ray images taken of a) crystal A and b) crystal B inside the crucible after growth was ended; c) numerically calculated shear stress in wafer A1 and B1 cut from crystals A and B, respectively.

We can approximate the impact of the reduced seed holder's thickness on the bow of the grown crystal by calculating the bow of the seedholder/seed stack after heating up to growth temperatures. The graphite seed holder will expand more than the SiC seed, therefore inducing a concave bow of the stack. If the seed holder's thickness increases, the bow will increase as well. Once the growth process on this concave seed is finished and the crystal cools down, the crystal will relax into a convex shape. The bow of the seed for crystal A prior to growing equals 29 m while the seed with

the thinner seed holder would exhibit a bow of 50 m. Assuming that crystal A was grown with the reduced seed holder's thickness without the other improvements of the growth process (such as in case of crystal B), the basal plane of the hypothetical resulting crystal A would display a bow of 16 m instead of 12 m. This would be the case if the seed holder completely relaxes and bends the crystal. In reality, the impact of the seed holder on the bow will most likely be lower. The additional increase of the bow's radius to 26 m as observed in wafer B1 is therefore presumed to be a result of the modification of the hot zone.

If the adjustments of the hot zone are implemented individually in the numerical simulation, we can approximate the impact of the adjustments. Only reducing the temperature gradients led to a decrease of the maximum stress in the resulting crystal by 6.1 MPa or 34% while reducing the thickness of the seed holder decreased the present maximum stress by 2.1 MPA or 12%. Finally, preventing a contact of the crystal to the graphite wall decreases the maximum stress by 1.8 MPA or 9%. It has to be mentioned that, considering the fact that the overall growth temperature and pressure was set to similar values and the axial temperature gradient was reduced, the growth rate of crystal B only amounted to 90 µm/h compared to 172 µm/h of crystal A. This additionally changed parameter has to be acknowledged. Generally, a higher crystal quality at lower growth rates has been reported. Sanchez et al. reduced the growth rate by increasing the ambient pressure and reported a decreased dislocation density [11]. Since the growth pressure was changed instead of the temperature gradients or the growth temperature itself, this effect of a decreased dislocation density should have mainly been caused solely by the growth rate. While adjusting the growth pressure is less impactful than changing the thermal conditions, it will still change the process conditions by changing the C/Si ratio in the gas phase due to different diffusion coefficients of the three main gas species Si, SiC_2 and Si_2C. A higher ambient pressure leads to a decreased C/Si ratio, which is known to decrease the crystal quality [12, 13]. Since Sanchez et al. reported higher crystal qualities at higher growth pressures, the beneficial effect of a slower growth rate seems to be more impactful than the unfavorable C/Si ratio. Therefore, it is to be expected that the lower growth rate due to the decreased axial temperature gradients further improved the crystal quality, in addition to the measurements undertaken in this work.

It can be concluded that by reducing the shear stress acting on the growing crystal, it is possible to completely suppress the formation of BPD arrays. This can be done by reducing the axial and radial temperature gradients, closely controlling the nitrogen doping during growth and reducing stress introduced by graphite parts such as the seed holder or the crucible wall. The reduction of the temperature gradients has to be implemented carefully. Reducing the axial gradient will also reduce the growth rate, if the overall growth temperature and pressure is kept the same, therefore a balance between growth rate and stress has to be found. The radial gradient must not be reduced too much, otherwise a concave growth interface will develop, leading to polytype switches and increased defect densities. The fact that crystal B exhibits not a single BPD array despite exhibiting residual amount of stress (seen in the appearance of BPDs and wafer bow) suggests that the stress acting on crystal B lies below a critical value needed to induce the formation of such arrays.

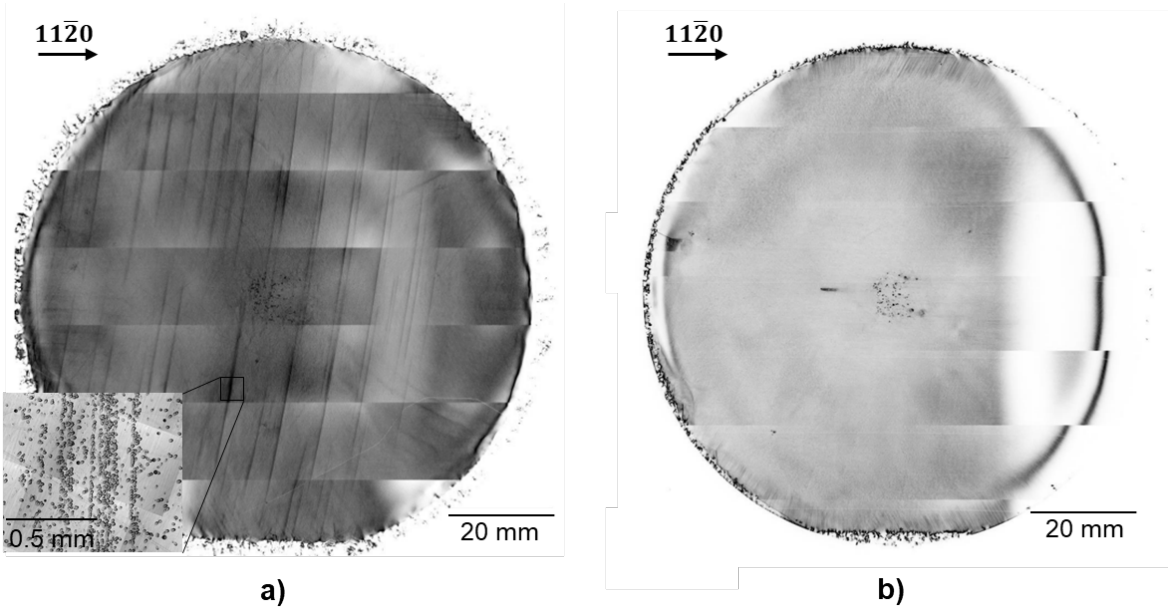

Fig. 2. XRT measurements taken with the 11$\bar{2}$0 reflex of a) wafer A1 and b) wafer B1. While wafer A1 exhibits bunched BPD-arrays, no arrays can be observed in wafer B1. The inset in wafer A1 depicts a magnified area of the bunched BPD array after being KOH-etched.

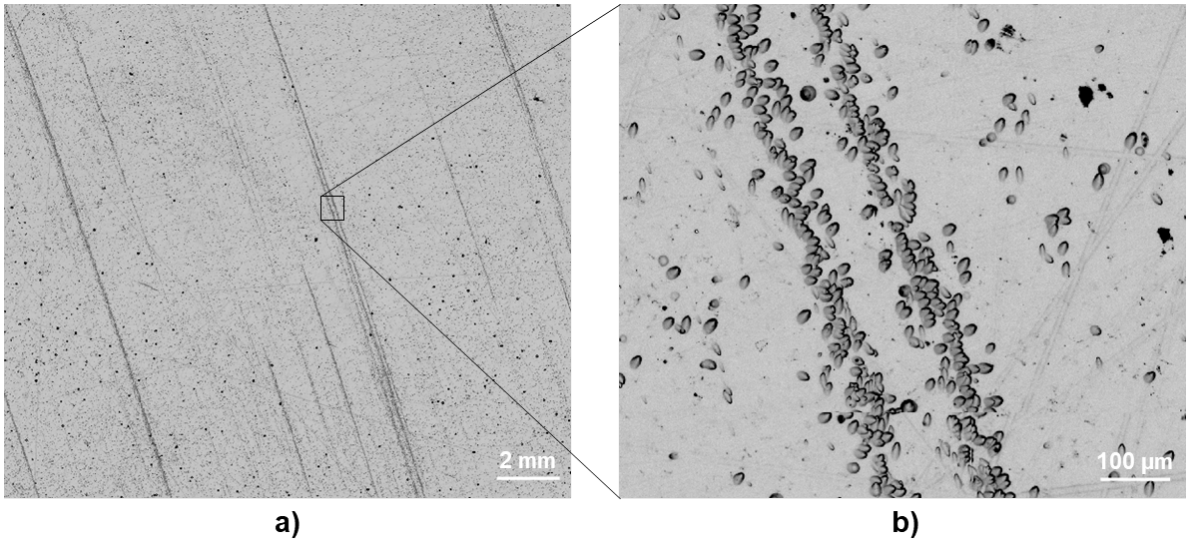

Fig. 3. Microscopic image of the KOH-etched surface of wafer A1.

Summary

We investigated the influence of hot zone modifications on the appearance of BPD arrays. As a result of the modifications of the growth cell, no bunched BPD arrays could be observed in case of crystal B, as demonstrated in XRT-measurements. The wafer bow was decreased, increasing the bow radius from 12 m to 26 m in the optimized growth run. The numerical calculations predicted a reduction of shear stress by 54% in the wafers close to the crystal cap from a maximum value of 18.0 MPa in wafer A1 to 8.3 MPa in wafer B1. The critical value of stress for the introduction of bunched BPDs and the periodicity of the BPD arrays should lie between those stress and wafer bow values. It was demonstrated that these collective adaptions to the growth cell can be applied to completely prevent the formation of any bunched BPD arrays.

Acknowledgments

XRT measurements were carried out by Dr. Christian Kranert in the service lab of the Fraunhofer department IISB in Erlangen (Germany). The funding by the DFG under the contract numbers WE2107-15 and SA2292-6 is greatly acknowledged.

References

[1] P. Wellmann, N. Ohtani, R. Rupp, *Wide Bandgap Semiconductors for Power Electronics*. 2021, Weinheim, Germany: Wiley-VCH.

[2] A. Agarwal, H. Fatima, S. Haney and S.-H. Ryu, A New Degradation Mechanism in High-Voltage SiC Power MOSFETs, IEEE Electron Device Letters 28(7) (2007) 587-589.

[3] V. Veliadis, H. Hearne, E.J. Stewart, M. Snook, W. Chang, J.D. Caldwell, H.C. Ha, N. El-Hinnawy, P. Borodulin, R.S. Howell, D. Urciuoli, A. Lelis and C. Scozzie, Degradation and Full Recovery in High-Voltage Implanted-Gate SiC JFETs Subjected to Bipolar Current Stress, IEEE Electron Device Letters 33(7) (2012) 952-954.

[4] M. Sonoda, T. Nakano, K. Shioura, N. Shinagawa and N. Ohtani, Structural characterization of the growth front of physical vapor transport grown 4H-SiC crystals using X-ray topography, J. Cryst. Growth 499 (2018) 24-29.

[5] N. Ohtani, M. Katsuno, T. Fujimoto, M. Nakabayashi, H. Tsuge, H. Yashiro, T. Aigo, H. Hirano, T. Hoshino and W. Ohashi, Analysis of Basal Plane Bending and Basal Plane Dislocations in 4H-SiC Single Crystals, Jpn. J. Appl. Phys. 48(6) (2009).

[6] T. Nakano, N. Shinagawa, M. Yabu and N. Ohtani, Formation and multiplication of basal plane dislocations during physical vapor transport growth of 4H-SiC crystals, J. Cryst. Growth 516 (2019) 51-56.

[7] B. Gao, K. Kakimoto, Three-Dimensional Modeling of Basal Plane Dislocations in 4H-SiC Single Crystals Grown by the Physical Vapor Transport Method, Crystal Growth and Design 14(3) (2014) 1272-1278.

[8] J. Steiner, P.J. Wellmann, Impact of Mechanical Stress and Nitrogen Doping on the Defect Distribution in the Initial Stage of the 4H-SiC PVT Growth Process, Materials 15(5) (2022).

[9] S. Nakashima, T. Kitamura, T. Mitani, H. Okumura, M. Katsuno and N. Ohtani, Raman scattering study of carrier-transport and phonon properties of4H−SiCcrystals with graded doping, Physical Review B 76(24) (2007).

[10] M. Stockmeier, R. Muller, S.A. Sakwe, P.J. Wellmann and A. Magerl, On the lattice parameters of silicon carbide, J. Appl. Phys. 105(3) (2009).

[11] E.K. Sanchez, J.Q. Liu, M. De Graef, M. Skowronski, W.M. Vetter and M. Dudley, Nucleation of threading dislocations in sublimation grown silicon carbide, J. Appl. Phys. 91(3) (2002) 1143-1148.

[12] M. Arzig, U. Künecke, M. Salamon, N. Uhlmann and P.J. Wellmann, Influence of the growth conditions on the formation of macro-steps on the growth interface of SiC-Crystals, J. Cryst. Growth 576 (2021).

[13] M. Arzig, U. Künecke, M. Salamon, N. Uhlmann and P.J. Wellmann, Analysis of the Morphology of the Growth Interface as a Function of the Gas Phase Composition during the PVT Growth of Silicon Carbide, Materials Science Forum 1062 (2022) 89-93.